STRESS STATE ANALYSIS OF SUB-SIZED PRE-CRACKED THREE-POINT-BEND SPECIMEN

Luděk Stratil*, Vladislav Kozák**, Hynek Hadraba**, Ivo Dlouhý*

The contribution deals with finite element analysis of stress state in sub-sized pre-cracked three-point bend specimen (KLST). A studied material was Eurofer'97 steel. The true stress-true strain curve was obtained from tensile test. The three-point-bend tests were carried out on pre-cracked plain and side-grooved specimens at ambient temperature. Performed tests were simulated using FEA software ABAQUS 6.10. The stress state in KLST specimen was compared with the stress state of pre-cracked Charpy and 1T SENB. The analysis confirmed the stress state in KLST specimens at the crack tip does not correspond to the stress state of standard fracture toughness determination because loss of crack-tip and out-of-plane constraint.

Keywords: *KLST, three-point bending, side grooving, Eurofer'97, J-integral*

1. Introduction

The determination of valid values of the fracture toughness usually requires using standard test specimens, which have sufficient dimensions to maintain the plain strain conditions. However, there are certain cases, where is not enough test material available for use of standard test specimen. The test specimens with dimensions smaller than standard one are called sub-sized specimens. The motivation for using sub-sized specimens can be found in amount of test material, possibility to characterize fracture behaviour locally, e.g. in weld joint. The use of small specimen is also necessary for development of materials in future fusion and fission applications due to both limited space and high heating rates in available irradiation facilities [1]. There are various types of sub-sized test specimen, but the most common for determination of fracture toughness are miniature and/or disc shaped compact tension specimens (CT) [2] and three-point-bend specimens (3PB). The latter are represented by pre-cracked Charpy, the half of pre-cracked Charpy and KLST type of test specimen. The KLST test specimen is the smallest of them with dimensions $3\times4\times27\,\mathrm{mm}^3$. Several variations of KLST specimens are used e.g. specimens for impact testing with V or U notch [3] or pre-cracked specimens [1, 4]. Small dimensions of KLST produce loss of constraint both in plane and out of plain and, in addition to, statistical size effect. This makes interpretation of the test results measured on sub-sized samples difficult in comparison with standard specimens. Owing to small thickness (3 mm), the crack tip stress state in KLST specimens is significantly influenced by close distance of its free surfaces and thus by the plane stress

* Ing. L. Stratil, prof. Ing. I. Dlouhý, CSc., Institute of Physics of Materials, ASCR, Group of Brittle Fracture; Žižkova 22, 616 62 Brno, Czech Republic and Institute of Material Science and Engineering, Faculty of Mechanical Engineering, Brno University of Technology, Technická 2896/2, 616 69, Brno, Czech Republic

** Ing. V. Kozák, CSc., Ing. H. Hadraba, Ph.D., Institute of Physics of Materials, ASCR, Group of Brittle Fracture; Žižkova 22, 616 62 Brno, Czech Republic

condition. Plastic flow reaches easily the surface of specimen bringing stress relaxation and generating lower stress level in crack tip process zone. The described stress relaxation cause, in the case of narrow thin specimens, the crack tunnelling effect [5]. The crack propagates preferentially in central part of specimens [5, 6]. If such specimen side-grooved the crack tunnelling effect vanishes and crack tip front is more uniform. The stress state in the specimen varies also with length of the crack. The triaxiality level in the body with shallow crack is lower than for deep cracked geometry.

The aim of this study is to quantify the stress state in plain and side-grooved KLST specimens with various crack length (a/W). The comparison of the stress state at the crack tip between the most used three-point-bend specimens, pre-cracked Charpy, standard 1T specimen and KLST specimen is presented.

2. Constraint effects

The stress state in the specimen generally depends on the test conditions, namely loading level, loading rate, test temperature and on specimen geometry. Particularly, the alloys with BCC (Body Centered Cubic) lattice perform strong temperature and loading rate dependence of yield stress. With decreasing temperature and increasing loading rate the yield stress increases. By keeping previous conditions constant there is also the influence of the specimen geometry, e.g. dimension, notch/crack geometry configuration. The crack tip constraint should be evaluated in order to describe and handle with all the effects mentioned above. The crack tip constraint can be described as limited extent of plastic deformation at the crack tip by surrounding amount of elastic loaded material. The structure with high level of constraint maintains high triaxiality level and vice versa. In the three dimensional body the plastic deformation is spaced in the volume of material. Relating to specimen dimensions and crack/specimen configuration the effect of constraint on plastic deformation can be concluded as in-plain constraint and out-of-plane constraint. The former type can be explained as the effect of unbroken ligament and the latter as the effect of specimen thickness on the stress triaxiality level at the crack tip. Because of three-dimensional nature the quantifications of individual constraint effects are not easy to distinguish [7]. When external conditions significantly affect the stress level at the crack tip, crack tip stresses relax, plastic strain field increases and the constraint loss occurs. This effect develops more rapidly in specimens with shallow cracks. In low constrained geometries or at high loading level, where the constraint loss occurs, the constraint effects associated with deviation from small scale yielding (SSY) can be evaluated [5, 8]. Moreover within certain conditions of constraint loss those can be corrected to the conditions corresponding to SSY. A number of micromechanical models have been used to solve those problems for ferritic steels fractured by cleavage initiation in the transition region [1, 5, 8]. These models generally combine simulation of crack-tip stress fields with local micromechanical models of damage. Newly it was shown that also for ductile fracture the constraint effect can be evaluated. Zhou has shown that the constraint parameters can be effectively used for obtaining R-curve under low-constraint level [9].

3. Mechanical Testing

A studied material was Eurofer'97 steel type of RAFM (Reducted Activation Feritic-Martensitic) developed for structural applications relating to fusion reactor. The nominal chemical composition of the steel is (in wt. %) 0.1 % C, 9.0 % Cr, 1.0 % W, 0.2 % Ta, 0.1 % V. Tensile tests were carried out to obtain true stress-true strain curve of the material. The tensile test was performed on plain specimen with diameter 4 mm and gauge length 20 mm according [10]. The tensile specimen was loaded quasistatically by loading rate 2 mm min^{-1} on test machine ZWICK Z50. The elongation of specimen was measured by external extensometer. For bending tests three geometries of pre-cracked KLST test specimens were prepared. The three-point-bend testing was preformed on test machine Instron 8862, taking into account standards [11]. The specimens were pre-cracked by cyclic loading on test machine MTS Tytron 250 to various ratio of crack length to width (a/W). In the first geometry the crack was introduced into half of specimen width ($a/W \sim 0.5$). The other two geometries possessed shorter cracks ($a/W \sim 0.35$). One of specimen with ratio $a/W \sim 0.35$ was side-grooved after cycling (Fig. 1). The specimens were loaded up to maximal load, during the test the deflection of specimens was measured. All mechanical tests were carried out at ambient temperature.

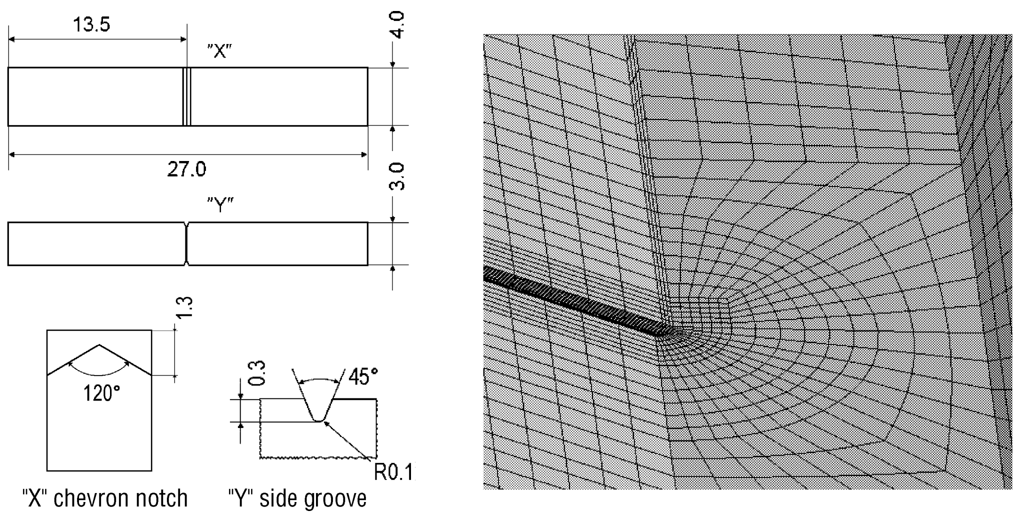

Fig.1: The geometry of KLST specimen (upper), geometry of the starting chevron notch and side-grooving (bottom left), dimensions in mm; the detail of FE mesh of side-grooved specimen (right)

4. Finite element modelling

The software ABAQUS 6.10 was used for finite element modelling. The true stress-strain curve of the studied steel was introduced applying incremental theory of plasticity. The incremental curve was constructed by 26 lines connecting 25 points lying on true stress-true strain curve. Beyond the ultimate strength (plastic instability limit) the incremental curve was elongated up to 300 % deformation according angle which true stress-true strain curve maintain before reaching the ultimate strength. Axisymmetric model of half of the tensile specimen was created for verification of incremental curve. The model of tensile specimen consists of 940 elements type of CAX8R (axisymmetric eight-node element with reduced integration). Boundaries conditions were prescribed on the lower part of the model as restricted movement in Y direction ($Y = 0$) and as symmetry on the left side in X direction ($XSYMM = 0$). The tensile model was driven by displacement using nonlinear geometry.

The model was loaded up to final deformation ($\Delta l = 5\,\mathrm{mm}$) by 0.1 mm increments prescribed to the nodes in the upper part of the model. Because the only half of tensile specimen was modelled, half-values of displacement were applied to the model. The force vs. displacement dependence was obtained on the basic of reaction forces from the upper part of model Fig. 2. The comparison of measured and modelled curves from Fig. 2 indicate suitability of applied material curve.

The 3D models of the three KLST specimens were built in configurations described above (Fig. 1). Using symmetry only one quarter of specimen was modelled. In dependence on the specimen geometry the models consisted from 30×10^3 to 40×10^3 elements of C3D8 and C3D20R type. The C3D8 and C3D20R are solid eight-node element and solid twenty-node element with reduced integration, respectively. The supports and loading pin were modelled as an analytical surface. The prescribed contacts were surface to surface type. To compare the stress state in KLST specimen with other usually used specimen geometry, models of standard and Charpy specimen were created. The models of pre-cracked standard and Charpy type specimen with crack length keeping ratio $a/W = 0.5$ were modelled by the same way as KLST specimens consisting of 39×10^3 and 28×10^3 elements, respectively. All models described above were also driven by displacement using nonlinear geometry. Due to nonlinear behaviour of the models the values of J-integral were evaluated for individual loading states. The domain contour integral for evaluation of values of J-integral was used [12].

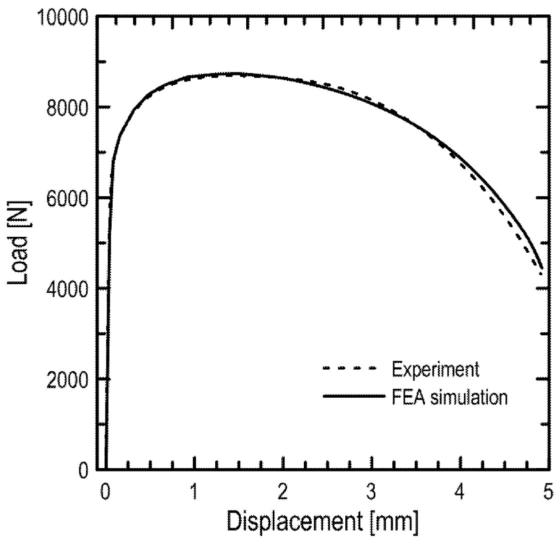

Fig.2: Comparison of measured and modelled force-displacement curves

5. Results

The Eurofer'97 steel demonstrated fully ductile behaviour at ambient temperature. Three curves load vs. deflection obtained from testing of KLST specimens are shown in Fig. 3. The specimens with shorter cracks ($a/W = 0.35$) are loaded to higher forces than specimens with standard crack length ($a/W = 0.5$) at the same deflection. It is because that specimens with shorter cracks have longer ligament (the unbroken part of material beneath the crack tip) and thus larger cross-section. Hence, loading of specimen with larger cross-section involves higher force. That can be also seen comparing curves for specimens with shorter cracks. In the case of side-grooved specimen, its cross-section is reduced by lateral notches. The side-grooved specimen has smaller cross-section than plain one and opens earlier and at lower forces. Results obtained from FEA (dashed) are also shown in the same figure. Experimentally determined and modelled load vs. deflection curves are identical only up to certain level of deflection. The locations where the calculated curves deviate from those experimentally determined are marked by arrows. No damage model was applied for FEA. That is why, load vs. deflection curves are corresponding to experimental ones, when damage does not take place. The deviation from measured curve could be connected with the onset of the crack growth. In the case of plain specimens, the measured and modelled curves are identical up to deflection about 0.4 mm, whereas for side-groove specimen just to deflection about 0.2 mm. The earlier deviation of measured and modelled curve for side-groove specimen is probably connected with earlier onset of ductile crack growth. The differences between used elements were observed. Although more time-demanding, the elements of the type C3D20R showed better computational performance than C3D8 elements when modelling large deflections. The use of eight-node elements for large deflection calculations caused unrealistic deformation of loaded curves. That was the reason why twenty-node elements were mainly used for computations.

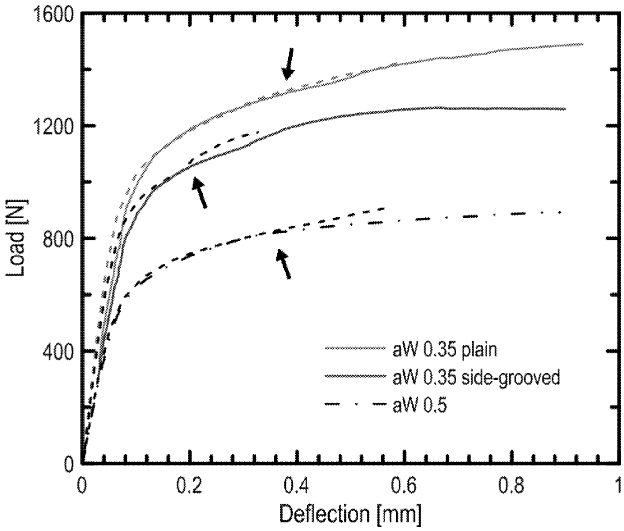

Fig.3: Measured load vs. deflection curves of KLST specimens and their FE simulation (dashed)

In the experimental part of the study the models of standard and pre-cracked Charpy specimen were created for comparison with KLST specimen. To do this, the distributions of maximal principal stress (MPS) ahead of the crack tip in the middle of the specimens were obtained from the models loaded to the same value of J-integral. The distributions of MPS are shown in Fig. 4 as the ratio of MPS to yield stress and loading parameter represented by relation $r\,\sigma_0/J$. The non-dimensional loading parameter $r\,\sigma_0/J$ is composed of the unbroken distance below crack tip r [mm], yield stress σ [MPa] and J-integral [MPa.mm]. The curve of MPS for standard specimen has maximum approximately in $r\,\sigma_0/J = 1$ and then decreases smoothly. The shape of MPS for standard specimen could be assumed to be very close to

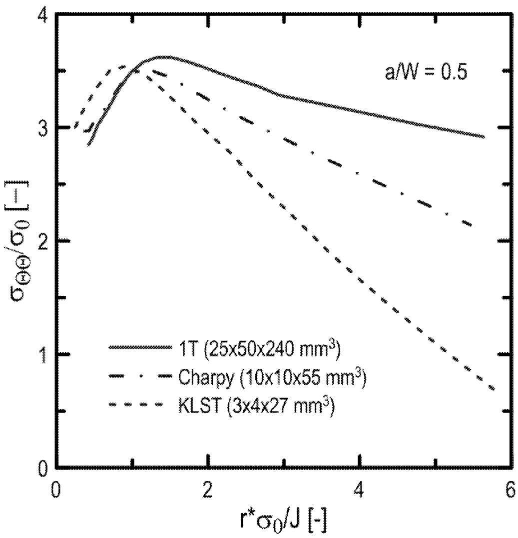

Fig.4: Comparison of curves of MPS at the crack tip in the middle of specimens

the plane strain conditions (i.e. conditions corresponding to SSY). Other specimens revealed different shape of MPS distribution. The maximums of MPS distributions for pre-cracked Charpy and KLST specimens are reached in lower distance from the crack tip and then substantial decrease is observed. The biggest decrease is observed for KLST specimens. The reduction of the stress fields at higher loading parameter is known as constrain loss and is quantified for $r\,\sigma_0/J = 2$ [2, 5]. The decrease of the MPS is result of larger plastic flow at the crack tip. The MPS distribution for KLST and also for pre-cracked Charpy specimen is not comparable with the MPS distribution of standard specimen. This leads to conclusion that under the tested conditions (ambient temperature, conditions of loading) the stress-state in sub-sized KLST specimen does not correspond to the plane strain conditions. Pre-cracked Charpy specimen seems to suffer less by the constraint loss than KLST specimen. One may found observed graduation of constraint loss in different ligament size, which is in modelled conditions 5 mm and 2 mm for pre-cracked Charpy and KLST specimen, respectively. However, these specimens have also different thicknesses and that is why the constraint loss is rather connected with different cross-sections below the crack. According to the work of Vlček, during the loading of the specimen first out-of-plane constraint and then in-plane constraint is developed [7]. Both types of constraint can be distinguished when keeping constant one dimension of specimen cross-section.

The distribution of MPS ahead the crack tip for tested KLST specimens is in Fig. 5. Although the specimens have different crack length, they maintain the same stress level. It seems that the different crack length in this case does not affect the stress level at the crack tip. It is in accordance with Chlup, who observed slight increase of stress at the crack tip only for shorter crack with $a/W = 0.2$ [13, 14]. For specimen with standard crack length the MPS level is decreasing more in the higher distance from the crack tip. It was found that shorter ligament was responsible for that decrease. During the loading the stresses change gradually across ligament from tensile at the crack tip to compressive at a contact side of specimen. In the specimen with shorter crack, the transition from tensile to compressive

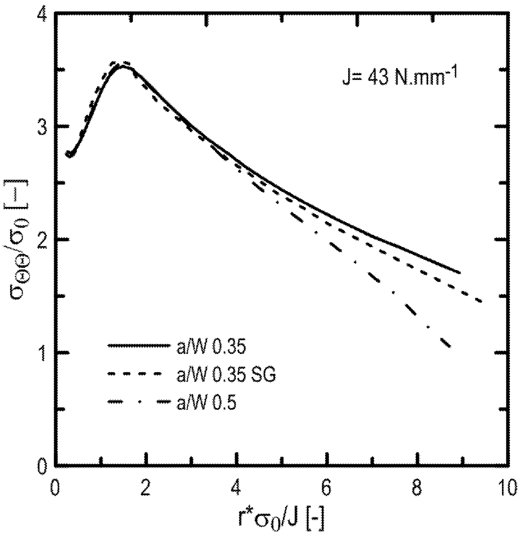

Fig.5: The MPS distribution in the middle of the KLST specimens with different ligament

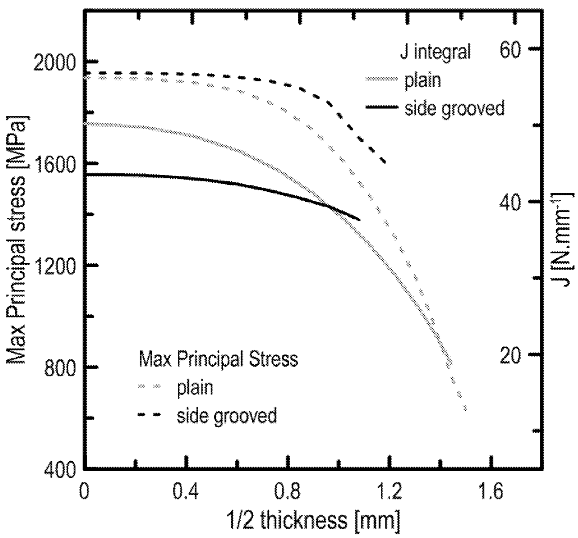

Fig.6: The MPS distributions and J-integral level along thickness in KLST specimens

MPS is smoother and hence, decrease of the stresses in the higher distance from the crack tip is slower. Regarding the stress distribution across the specimen, the longer ligament seems to be more suitable for longer crack propagation and thus for purposes of R-curve evaluation.

The effect of the side-grooving on the stress state in KLST specimens could be followed from Fig. 6. The MPS distributions at the crack tip in the middle part were identical both for plain and side-grooved specimen. For side-grooved specimen the MPS distribution is quite uniform along thickness except for locations close to the side notch root where decreases. The shape of MPS distribution for plain specimen is different, the MPS is decreasing continuously in direction to the surface and the difference of the stress level is substantial when comparing the middle and surface part of the specimen. The distributions of total values of J-integral along thickness have same trends as MPS distributions. To obtain J-integral value of the specimen corresponding to that experimentally determined, the local numerically determined J-values must be averaged along the crack tip of specimen thickness. The mean value of J-integral for side-grooved specimen averaged along the thickness appears to be $42.1\,\mathrm{N\,mm^{-1}}$. This is in good accordance with the value experimentally determined $44.7\,\mathrm{N\,mm^{-1}}$. In the case of plain specimen, the mean value of the J-integral determined by this way was $40.9\,\mathrm{N\,mm^{-1}}$, which is also well comparable with experimentally determined value $42.0\,\mathrm{N\,mm^{-1}}$. The agreement between numerically and experimentally determined values of J-integral was within 6 % and 3 % scatter for side-grooved and plain specimen, respectively.

6. Conclusion

KLST specimens were tested having different a/W ratio and in addition with and without side grooving. The FEA was applied to obtain the maximal principal stress distribution below the crack tip in experimentally tested specimen geometries and also in the pre-cracked standard and pre-cracked Charpy type specimens. Stress state in the KLST specimen in tested conditions (ambient temperature, conditions of loading) does not correspond to the plane stress conditions needed for fracture toughness determination. The side grooving helps to maintain the stress level at the crack tip along the thickness however it does not have influence on the maximum value of the stress. The agreement between numerically and experimentally determined values of J-integral was within 6 % and 3 % scatter for side-grooved and plain specimen, respectively.

Acknowledgement

The authors gratefully thanks for the financial support of projects of the Czech Science Foundation No. 107/10/0361 and 106/09/H035.

References

[1] Yamamoto T., Odette G.R., Sokolov M.A.: On the fracture toughness on irradiated F82H: Effects of loss of constraint and strain hardening capacity, J. Nucl. Mater., Vol. 417, Issue 1–3, pp. 115–119
[2] Maloy S.A., et. al.: The mechanical properties of 316/304L stainless steels, Alloy 718 and Mod 9C-1Mo after irradiation in a spallation environment, J. Nucl. Mater., Vol. 296, 2001, pp. 119–128
[3] DIN50115: Notched bar impact testing of metallic materials using test pieces other than ISO test pieces, Deutsches Institut Fur Normung E.V. (German National Standard) /01-Apr-1991/ 3 pages
[4] Gaganidze E., Dafferner J., Aktaa J.: Scientific report FZKA 7252, Forschungszentrum Karlsruhe, Karlsruhe 2006
[5] Anderson T.L.: Fracture Mechanics Fundamentals and Applications, Second Edition, CRC Press, 1995
[6] Schenider H.-C., Aktaa J., Rolli R.: Small fracture toughness specimen for post-irridiation experimensts, J. Nucl. Mater., 599, 2007, 367–370
[7] Vlček L.: Numerická 3D analýza těles s trhlinou, IPM ASCR Brno, 2004
[8] Nevalainen M., Dodds R.H.: Numerical studies of 3-D constraint effects on brittle fracture in SE(B) and C(T) specimens, Int. J. Frac. 74, 1995, 131–161

[9] Zhou D.W.: Measurement and modelling of R-curves for low-constraint specimens, Engng. Fract. Mech., Vol. 78, Issue 3, 2011, pp. 605–622
[10] ČSN EN 10002-1 Metallic materials – Tensile testing – Part 1: Method of test at ambient temperature
[11] ISO 12135:2002(E) – Metallic materials – Unified method of test for the determination of quasistatic fracture toughness
[12] Hibbit, Karlsson, Sorensen, ABAQUS Users Manual: Version 6.5, Inc., 2005
[13] Chlup Z., Dlouhý I.: Micromechanical aspects of constraint effect at brittle fracture initiation, 65–78, Transferability of Frac. Mech. Characteristic, I. Dlouhý, Kluwer Academic Publisher, 2002, ISBN 978-1-4020-0794-1
[14] Dlouhý I., Chlup. Z., Kozák V.: Constraint effects at brittle fracture initiation in a cast ferritic steel, Engng. Fract. Mech., 71, 2004, 873–883

Received in editor's office: July 7, 2011
Approved for publishing: May 17, 2012